RSC Advances

Journal Name

ARTICLE

Color-Tunable Emission in Ce^{3+}, Tb^{3+} Co-doped $Ca_5(BO_3)_3F$ Phosphor

Received 00th January 20xx,
Accepted 00th January 20xx

DOI: 10.1039/x0xx00000x

www.rsc.org/

Liping Yi,[a, b] Jilin Zhang,*[a, b] Zhongxian Qiu,[a, b] Wenli Zhou,[a, b] Liping Yu[a, b] and Shixun Lian*[a, b]

In this paper, Ce^{3+} doped and Ce^{3+}, Tb^{3+} co-doped $Ca_5(BO_3)_3F$ phosphors were synthesized by a high-temperature solid-state reaction. Upon excitation at 360 nm, the emission spectra of Ce^{3+} doped phosphors exhibit a broad emission band peaking at 392 nm, which originates from 5*d* to 4*f* transition of Ce^{3+}. The Ce^{3+}, Tb^{3+} co-doped phosphors show strong energy transfer from Ce^{3+} to Tb^{3+}, and the emission color can be tuned from purplish blue to green by changing Tb^{3+} content. The excitation band in 300-400 nm region broadens when monitored at 541 nm compared to that monitored at 392 nm. Furthermore, the co-doping of Tb^{3+} facilitates the appearance of green emitting Ce^{3+}, which originates from Ce^{3+} on Ca site other than that for purplish-blue Ce^{3+}. The relationship between the luminescent properties of Ce^{3+} and its coordination environments, namely, different Ca sites, is discussed based on the calculations of centroid shift and crystal field splitting of 5*d* energy levels of Ce^{3+}. Results suggest that Ce^{3+}, Tb^{3+} co-doped $Ca_5(BO_3)_3F$ phosphors may be a candidate for near-UV chip based white light-emitting diodes.

1. Introduction

White light-emitting diodes (w-LEDs) have been regarded as the new generation of illumination source due to the numerous advantages, such as long lifetime, energy saving, environmental friendliness, etc, when they compare with the traditional incandescent and fluorescent lamps.[1-3] However, the commonly used w-LEDs at present, which are based on the combination of a blue InGaN LED chip and a yellow emitting $Y_3Al_5O_{12}:Ce^{3+}$ (YAG:Ce), have a low color rendering index (CRI, Ra < 80) and a high color temperature due to the lack of red-emitting component.[4, 5] These problems can be overcome by combining a near-UV LED chip with a white-emitting phosphor or blue, green and red emitting phosphors.[2, 6] Therefore, it is important to search phosphors that could be excited efficiently by near-UV LEDs.

Ce^{3+} ion is a common activator for phosphors with intense and broad excitation and emission bands due to the allowed 4*f*-5*d* and 5*d*-4*f* transitions, respectively, which is similar as Eu^{2+} ion. Furthermore, the excitation and emission bands can be adjusted by changing hosts or crystallographic sites in a host.[7, 8] Therefore, it is quite convenient to obtain phosphors that are suitable for near-UV LEDs by selecting a proper host. In the past year, there were several new Ce^{3+} doped phosphors reported, such as, $BaLa_2Si_2S_8:Ce^{3+}$,[9] γ-$Ca_2SiO_4:Ce^{3+}$,[10] $MSiAl_2O_3N_2:Ce^{3+}$ (M = Sr, Ba),[11] novel garnet $Ca_2GdZr_2(AlO_4)_3:Ce^{3+}$,[12] and $Ca_{3-x}Sr_xAl_2O_6:Ce^{3+}$ (x = 0, 1 and 2),[8, 13, 14] etc.

Tb^{3+} ion is used as a green-emitting component of phosphors, which usually has an intense emission peak at ~540 nm originating from $^5D_4$-$^7F_5$ transition. However, the excitation bands in near-UV region are usually very weak due to the forbidden 4*f*-4*f* transitions. Therefore, Ce^{3+} and Eu^{2+} ions are utilized to enhance the emission intensity of Tb^{3+} by energy transfer.[15-26]

In the present work, we are going to report the luminescent properties of Ce^{3+} doped and Ce^{3+}, Tb^{3+} co-doped $Ca_5(BO_3)_3F$ phosphors. The emission color of the phosphors can be tuned from purplish blue to green by energy transfer from Ce^{3+} to Tb^{3+}. Furthermore, the excitation and absorption bands of the Ce^{3+}, Tb^{3+} co-doped phosphors broaden compared to the single-doped ones, which show potential application as phosphor for near-UV LEDs.

2. Experimental Section

$Ca_5(BO_3)_3F$: Ce^{3+}/Tb^{3+} Phosphors were prepared by a high-temperature solid-state reaction under a reductive atmosphere. In a typical synthesis procedure, raw materials $CaCO_3$ (A.R.), CaF_2 (A.R., excess 10%), H_3BO_3 (A.R., excess 3%), CeO_2 (4N) and Na_2CO_3 (A.R.) were thoroughly mixed with a hypothetical composition of $Ca_{5-2x}(BO_3)_3F$: xCe^{3+}, xNa^+ (CBOF: xCe^{3+}, xNa^+), where Na^+ acted as charge compensator. After ground thoroughly, the mixed raw materials were calcined in a tube furnace at 1000 °C for 6 h under a gas flow of 5% H_2 plus 95% N_2. The as-synthesized phosphors were ground and subjected to phase characterization and luminescent study.

[a.] Key Laboratory of Chemical Biology and Traditional Chinese Medicine Research (Ministry of Education of China), Hunan Normal University, Changsha 410081, China.
[b.] Key Laboratory of Sustainable Resources Processing and Advanced Materials of Hunan Province College, Hunan Normal University, Changsha 410081, China. Fax and Tel: +86 731 88865345; E-mail: chemzhangjl@hunnu.edu.cn (Jilin Zhang), sxlian@hunnu.edu.cn (Shixun Lian).

Raw material Tb_4O_7 (4N) is used as the source of Tb^{3+} ion. The amount of $CaCO_3$ is reduced for the substitution of luminescent centers. One should notice that the molar concentrations for Ce^{3+} and Tb^{3+} are 0.2*x* and 0.2*y*, respectively.

X-ray powder diffraction (XRD) patterns were collected by a Shimadzu X-ray Diffractometer XRD-6100 with Cu $K\alpha$ radiation at 40 kV and 30 mA with a scan speed of 8 degree/min. Photoluminescence (PL) and photoluminescence excitation (PLE) spectra of the phosphors were collected on a Hitachi F4500 spectrophotometer with a 150 W xenon lamp. Diffuse reflectance (DR) spectra were performed on a Hitachi U-3310 Spectrophotometer using $BaSO_4$ as a standard reference. Decay curves were recorded on an EDINBURGH FLS920 combined Fluorescence Lifetime & Steady State Spectrometer with a 450 W xenon lamp. The morphology and elemental mapping of samples were observed with a thermal field emission environmental SEM-EDS-EBSD (Quanta 400F). Ce and Tb elements on the surface of phosphors are detected by X-ray photoelectron spectroscopy (Thermo Scientific ESCALAB 250, USA). Transmission electron microscopic (TEM) micrographs and high resolution TEM (HR-TEM) images were obtained on a Tecnai G2 F20 S-TWIN electron microscope (America, FEI, 200 kV). All measurements were carried out at room temperature.

3. Results and Discussion

3.1 Phase Characterization, Crystal Structure and Morphology

The XRD patterns of selected CBOF: $x$$Ce^{3+}$, $x$$Na^+$ and CBOF: $0.03Ce^{3+}$, $y$$Tb^{3+}$, $(0.03 + y)Na^+$ phosphors are shown in Figure 1 together with standard PDF cards. When the doping contents of Ce^{3+} or Tb^{3+} are low, the samples contain mainly $Ca_3(BO_3)_3F$ phase (PDF#80-1702) and an impurity phase, namely, CaO (PDF#75-0264). The diffraction intensity of CaO peaks weakens gradually and finally disappears as the increase of Ce^{3+} or Tb^{3+} content (see Figure 1d). We attempted to avoid the formation of CaO by reducing the amount of $CaCO_3$ raw material. The diffraction peaks of CaO weaken indeed, however, additional peaks that belong to $Ca_3(BO_3)_2$ appear. Fortunately, the luminescent properties of CaO: Ce^{3+}, Na^+ can be distinguished from that of CBOF: Ce^{3+}, Na^+, which will be discussed below. The crystal structure of $Ca_5(BO_3)_3F$ is illustrated in Figure 1e. $Ca_5(BO_3)_3F$ crystallizes in a monoclinic phase. There are three Ca crystalline sites, which are denoted as Ca(1), Ca(2) and Ca(3). Ca(1) coordinates with 5 O and 1 F, Ca(2) coordinates with 6 O, and Ca(3) coordinates with 4 O and 2 F. The numbers of Ca(1), Ca(2) and Ca(3) atoms in a unit cell are 4, 4 and 2, respectively.

The XRD analysis implies that Ce^{3+}, Tb^{3+} and Na^+ ions have entered into the lattice of the host. XPS and elemental mapping are also conducted to confirm the above assumption. Figure 2 shows the XPS results of Ce and Tb in CBOF: $0.03Ce^{3+}$, $0.15Tb^{3+}$, $0.18Na^+$. The binding energies of Ce $3d_{5/2}$, Ce $3d_{3/2}$ and Tb 4d are inconsistence with the reference data,[27] which indicates the existence of Ce and Tb in the final products. Elemental mapping was conducted by using SEM and EDS, in order to get the information of the distribution of these doping elements in the particles. The elemental maps of Ca, Ce, Tb and Na for corresponding particles of selected Ce^{3+}-doped, Ce^{3+} and Tb^{3+} co-doped phosphors are shown in Figure 3. Results indicate that the doping ions are well distributed in the particles.

The SEM images of three representative phosphors are shown in Figure 4. The morphologies of the phosphor particles are irregular with a size in micrometer region. Furthermore, the particle size increases with the amount of Na^+, which implies that Na_2CO_3 acts as not only the supplier of charge compensator (Na^+), but also fluxing agent. TEM and HRTEM images of selected Ce^{3+} doped and Ce^{3+}, Tb^{3+} co-doped phosphors are illustrated in Figure 5. The interplanar distances of (110) plane for these two phosphors are near the same, indicating the doping ions make little change to the crystal lattice of the host.

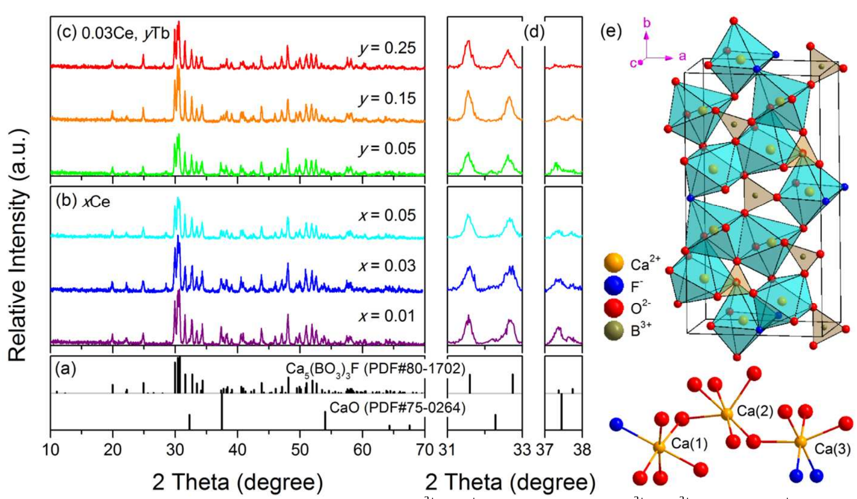

Figure 1. XRD patterns of (a) Stand PDF cards, (b) CBOF: $x$$Ce^{3+}$, $x$$Na^+$ and (c) CBOF: $0.03Ce^{3+}$, $y$$Tb^{3+}$, $(0.03 + y)Na^+$, (d) the magnified XRD patterns in 31-33° and 37-38° regions, (e) crystal structure of $Ca_5(BO_3)_3F$.

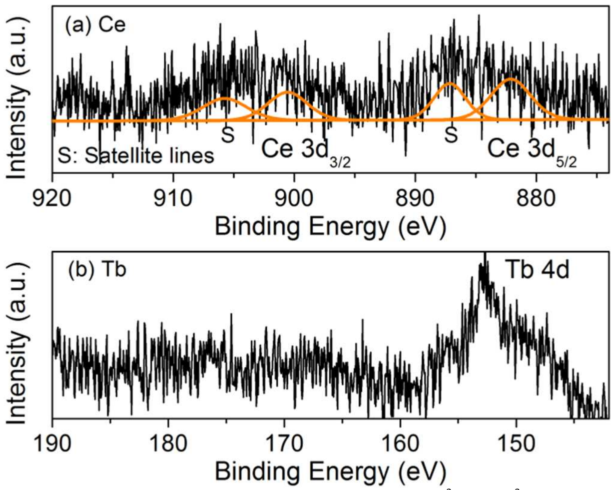

Figure 2. XPS spectra of (a) Ce 3d and (b) Tb 4d in CBOF: $0.03Ce^{3+}$, $0.15Tb^{3+}$.

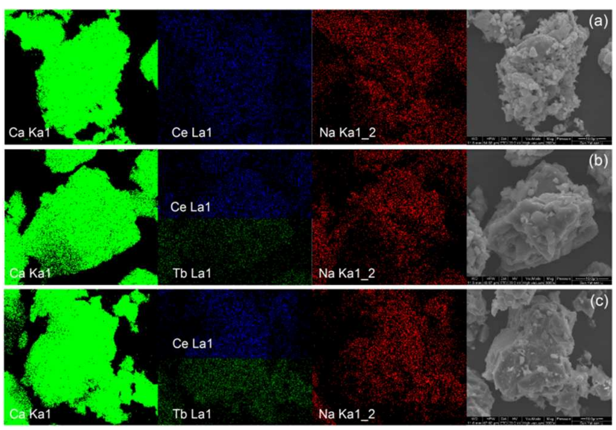

Figure 3. Elemental mapping of Ca, Ce, Tb and Na for corresponding SEM images of (a) CBOF: $0.03Ce^{3+}$, $0.03Na^{+}$, (b) CBOF: $0.03Ce^{3+}$, $0.05Tb^{3+}$, $0.08Na^{+}$ and (c) CBOF: $0.03Ce^{3+}$, $0.15Tb^{3+}$, $0.18Na^{+}$.

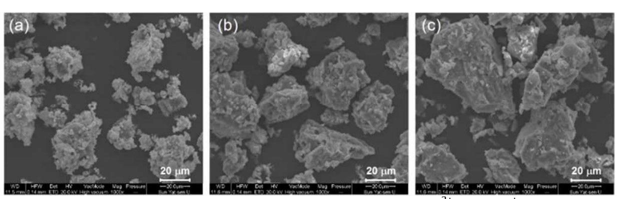

Figure 4. SEM images of selected phosphors. (a) CBOF: $0.03Ce^{3+}$, $0.03Na^{+}$, (b) CBOF: $0.03Ce^{3+}$, $0.05Tb^{3+}$, $0.08Na^{+}$ and (c) CBOF: $0.03Ce^{3+}$, $0.15Tb^{3+}$, $0.18Na^{+}$.

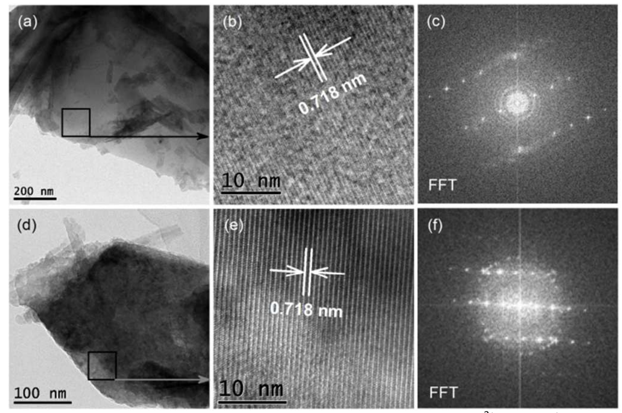

Figure 5. TEM and HRTEM images of phosphors: (a-c) CBOF: $0.03Ce^{3+}$, $0.03Na^{+}$ and (d-f) CBOF: $0.03Ce^{3+}$, $0.15Tb^{3+}$, $0.18Na^{+}$ (FFT: Fast Fourier Transform).

3.2 Luminescence Properties

The DR spectra of CBOF host, Ce^{3+}/Tb^{3+} single-doped and Ce^{3+}, Tb^{3+} co-doped phosphors are illustrated in Figure 6. There is a weak absorption band around 250 nm for the host. There are two obvious absorption bands peaking at ~340 and ~420 nm for CBOF: Ce^{3+}, Na^{+}. Furthermore, a weak band around 470 nm is deduced from the asymmetric band of 420 nm. For Tb^{3+} doped phosphor, there are several absorption bands in 200-330 nm region. While, the absorption bands for Ce^{3+}, Tb^{3+} co-doped phosphors seem the combination of those for Ce^{3+} and Tb^{3+} single-doped ones. Furthermore, the absorption intensities for Ce^{3+}, Tb^{3+} co-doped phosphors increase with Tb^{3+} content.

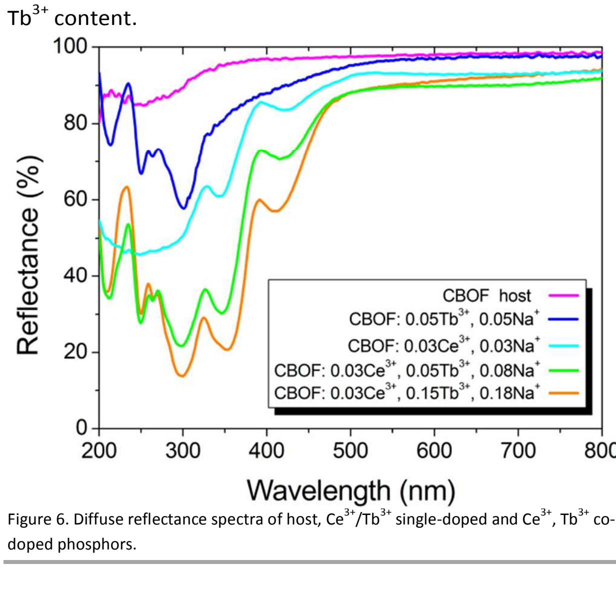

Figure 6. Diffuse reflectance spectra of host, Ce^{3+}/Tb^{3+} single-doped and Ce^{3+}, Tb^{3+} co-doped phosphors.

The PL and PLE spectra of CBOF: $0.03Ce^{3+}$, $0.03Na^{+}$ are illustrated in Figure 7. Firstly, the PL spectrum excited by a 360 nm light contains an asymmetric band peaking at 392 nm originating from 5*d* → 4*f* transition of Ce^{3+} (Figure 7a), suggesting a purplish-blue emission. The corresponding PLE spectrum in the 200-380 nm near UV region is composed of four bands at 250, 290, 338 and 360 nm. The strongest excitation band locates at 360 nm. Secondly, the PL spectra excited by 400 and 465 nm are also collected and shown in Figure 7b according to the DR spectra. There is no emission band when excited at 400 nm. While a broad emission band at 550 nm is observed when excited by a blue light around 460 nm, which is the same as that of CaO: Ce^{3+}, Na^{+} [28, 29]. This PLE and PL spectra, indeed, belong to CaO: Ce^{3+}, Na^{+}, which will be approved below by the luminescent properties of Ce^{3+}, Tb^{3+} co-doped samples. Figures 3c-f show the PL spectra excited by 250, 290, 338 and 360 nm lights, which indicate that the resulted emission bands peak at a same wavelength. All the emission bands contain two Gaussian fitted bands, with energy differences of 1539-1806 cm^{-1}, which are in consistent with the energy differences of 4*f* sublevels of Ce^{3+} due to spin-orbital coupling. Therefore, these four excitation bands, which are monitored at 392 nm, originate from the 4*f* → 5*d* transitions of Ce^{3+} ions on a same crystalline site. The curves of PL intensity versus Ce^{3+} content is illustrated in Figure 7a, which suggests that the optimal doping content (x) of Ce^{3+} is 0.03, namely, $Ca_{4.94}(BO_3)_3F$: $0.03Ce^{3+}$, $0.03Na^{+}$. The difference between DR and PLE spectra of Ce^{3+} doped phosphor suggests that the absorption of a light is not necessarily accompanied by emission of a light.

The PLE spectrum of CBOF: Tb^{3+}, Na^{+} monitored at 541 nm contains five bands at 241, 261, 272, 284 and 324 nm and two weaker peaks at 379 and 485 nm (see Figure 8a). DR spectrum of CBOF: Tb^{3+}, Na^{+} also exhibits 5 absorption bands in 200-350 nm region, one of which is on the shoulder of the band at 300 nm. By comparing the DR spectra of the host and CBOF: Tb^{3+}, Na^{+}, and the PLE spectrum of CBOF: Tb^{3+}, Na^{+}, it could be deduced that the five excitation bands of CBOF: Tb^{3+}, Na^{+} originate from 4*f* → 5*d* transitions of Tb^{3+}. While the excitation peaks at 379 and 485 nm belong to $^7F_6 \rightarrow {}^5D_3$ and $^7F_6 \rightarrow {}^5D_4$ of Tb^{3+}, respectively. Figure 8b shows again the PLE and PL spectra of CBOF: Ce^{3+}, Na^{+} for comparison. There is overlap between the PL spectrum of Ce^{3+} and the PLE spectrum of Tb^{3+}, suggesting the existence of energy transfer from Ce^{3+} to Tb^{3+}. The PLE spectrum of Ce^{3+}, Tb^{3+} co-doped CBOF phosphor monitored at 541 nm contains not only excitation bands from 4*f* → 5*d* and intra-4*f* transitions of Tb^{3+}, but also two broad bands in about 330-450 nm region as shown in Figure 8d, which are not the same as that monitored at 392 nm (Figure 8b,c). The Gaussian fitting result of the 300-450 nm band for CBOF: $0.03Ce^{3+}$, $0.30Tb^{3+}$, $0.33Na^{+}$ is illustrated in Figure 8d, which contains five Gaussian peaks at 324, 341, 362, 379 and 400 nm. Therefore, the 300-385 nm PLE band of Ce^{3+}, Tb^{3+} co-doped CBOF phosphors is the overlap of bands at 324 nm (Tb^{3+}), 338 nm (Ce^{3+}) and 360 nm (Ce^{3+}). The PLE band of Ce^{3+}, Tb^{3+} co-doped phosphors at ~400 nm exists neither in Tb^{3+} single-doped nor in Ce^{3+} single-doped CBOF phosphors.

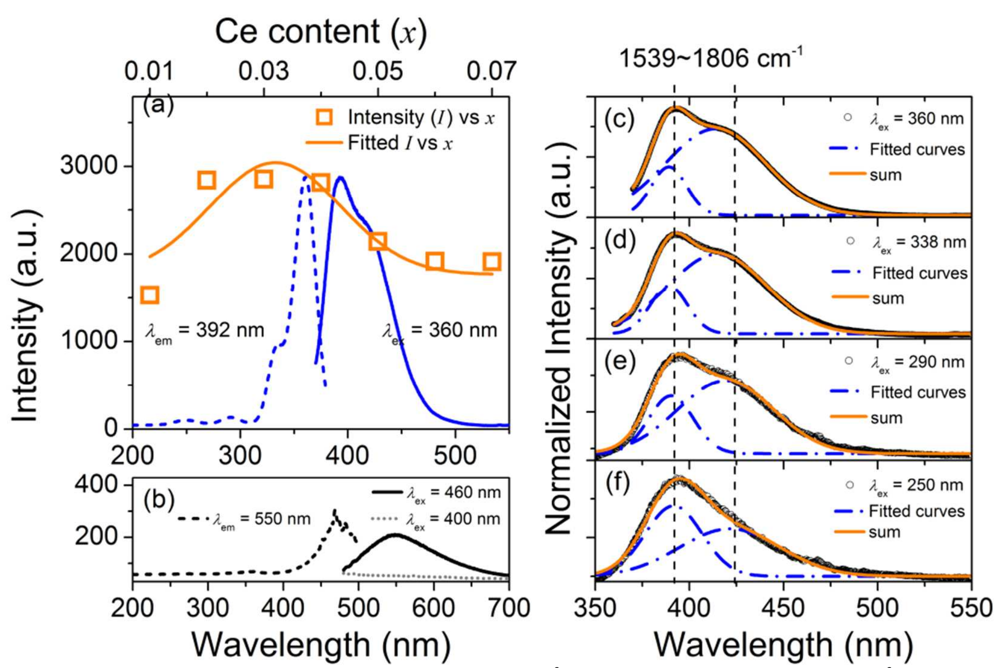

Figure 7. (a) PL (λ_{ex} = 360 nm) and PLE (λ_{em} = 392 nm) spectra of CBOF: $0.03Ce^{3+}$, $0.03Na^{+}$, and Curve of PL intensity versus Ce^{3+} content; (b) PL (λ_{ex} = 400, 465 nm) and PLE (λ_{em} = 550 nm) spectra of CBOF: $0.03Ce^{3+}$, $0.03Na^{+}$; (c-f) PL spectra under different UV lights and corresponding Gaussian fitted curves.

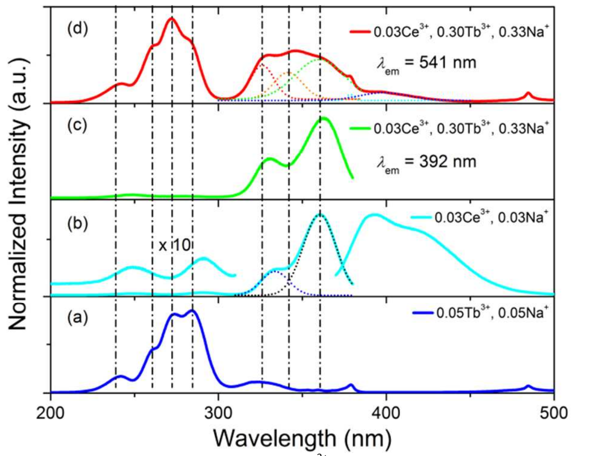

Figure 8. Comparison in PLE spectra of (a) Tb^{3+} single-doped CBOF phosphor (λ_{em} = 541 nm), (b) PL (λ_{ex} = 360 nm) and PLE (λ_{em} = 392 nm) of Ce^{3+} single-doped phosphor and (c,d) PLE of Ce^{3+}-Tb^{3+} co-doped CBOF phosphors.

The PL spectra of CBOF: $0.03Ce^{3+}$, yTb^{3+}, $(0.03 + y)Na^{+}$ excited by 360 nm light contain both the purplish-blue emission band of Ce^{3+} and the typical narrow emission bands of Tb^{3+} as shown in Figure 9a. The emission intensities of 392 nm band decrease with the increase of Tb^{3+} content (y), while those of Tb^{3+} bands increase firstly, reaching a maximum at y = 0.20, and then decrease. Figure 9b is the PLE spectra of Ce^{3+}, Tb^{3+} co-doped samples monitored at 541 nm. Intensities of all the PLE bands belonging to Ce^{3+} and Tb^{3+} in CBOF have similar tendencies as that of Tb^{3+} PL bands in co-doped samples. Figure 9c illustrates the PL intensities of Ce^{3+} (392 nm) and Tb^{3+} (541 nm) versus Tb^{3+} content in CBOF: $0.03Ce^{3+}$, yTb^{3+}, $(0.03 + y)Na^{+}$ for clarity. Figure 9d illustrates the CIE chromaticity diagram of CBOF: $0.03Ce^{3+}$, yTb^{3+}, $(0.03 + y)Na^{+}$ (y = 0 - 0.30) under 360 nm excitation and the photographs of corresponding phosphors under 365 nm lamp, indicating that the emission color of the phosphors can change from purplish blue to green with the increase of Tb^{3+} content. These results indicate that there is energy transfer from Ce^{3+} to Tb^{3+}.

Decay time curves of the Ce^{3+} single-doped and Ce^{3+}, Tb^{3+} co-doped samples monitored at 392 nm are illustrated in Figure 10. The decay time curve of CBOF: Ce^{3+}, Na^{+} is single exponential, while it changes to non-exponential for Ce^{3+}, Tb^{3+} co-doped ones, and the decay time shortens with the increase of Tb^{3+} content. The decay curves can be well fitted by the following equations[30]

For Ce^{3+} single-doped one,

$$I = A_1 \exp(-t/\tau_1) \quad (1)$$

For Ce^{3+}, Tb^{3+} co-doped ones,

$$I = A_1 \exp(-t/\tau_1) + A_2 \exp(-t/\tau_2) \quad (2)$$

where I is the luminescence intensity, t is the time, τ_1 and τ_2 are lifetimes, and A_1 and A_2 are constants. The average decay times (τ) can be calculated by the following formula[30]

$$\tau = (A_1\tau_1^2 + A_2\tau_2^2) / (A_1\tau_1 + A_2\tau_2) \quad (3)$$

The decay times decrease with the increase of Tb^{3+} as shown in Table 1 and Figure 10. These phenomena suggest the existence of energy transfer from purplish-blue emitting Ce^{3+} to Tb^{3+}. The energy transfer efficiency (η_T) from Ce^{3+} to Tb^{3+} can be calculated by the following equation[31]

$$\eta_T = 1 - \frac{\tau}{\tau_0} \quad (4)$$

where τ_0 and τ are the lifetimes of Ce^{3+} in the absence and presence of Tb^{3+}, respectively. The energy transfer efficiency can reach 45% when Tb^{3+} content (y) is 0.30 (Table 1).

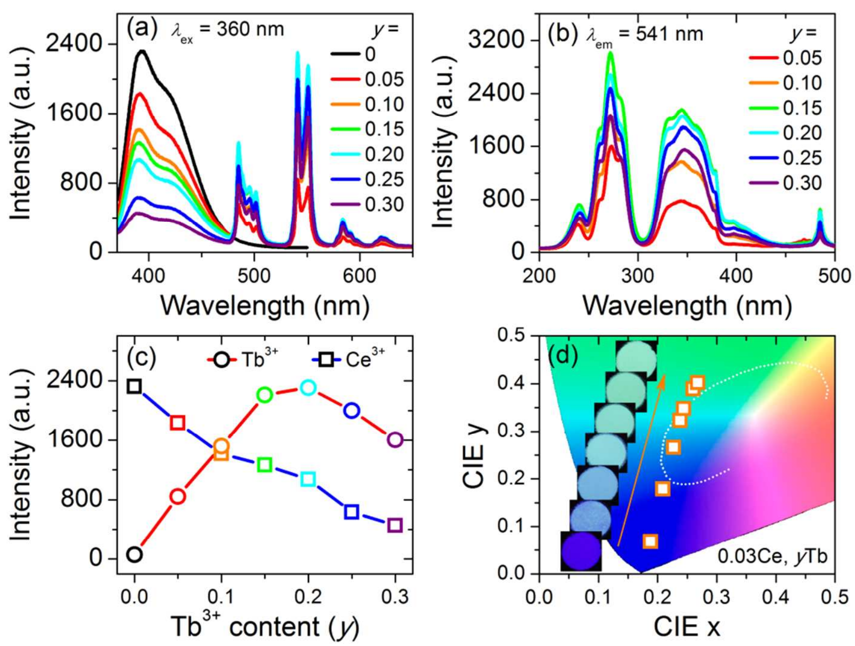

Figure 9. (a) PL (λ_{ex} = 360 nm) and (b) PLE (λ_{em} = 541 nm) spectra of CBOF: $0.03Ce^{3+}$, yTb^{3+}, $(0.03 + y)Na^{+}$; (c) PL intensities of Ce^{3+} (392 nm) and Tb^{3+} (541 nm) versus Tb^{3+} content (y); (d) CIE chromaticity diagram for CBOF: $0.03Ce^{3+}$, yTb^{3+}, $(0.03 + y)Na^{+}$ (y = 0 - 0.30) under 360 nm excitation, insert: photographs of phosphors under 365 nm lamp.

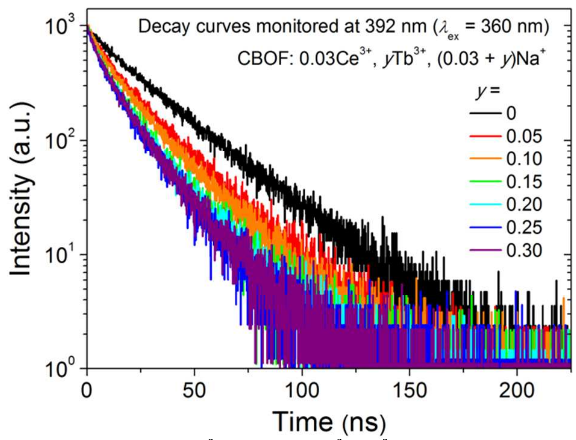

Figure 10. Decay curves of Ce^{3+} in CBOF: 0.03Ce^{3+}, yTb^{3+}, (0.03 + y)Na^+ phosphors monitored at 392 nm and excited by a 360 nm light. Insert shows the decay times and efficiencies of energy transfer from purplish-blue Ce^{3+} to Tb^{3+}.

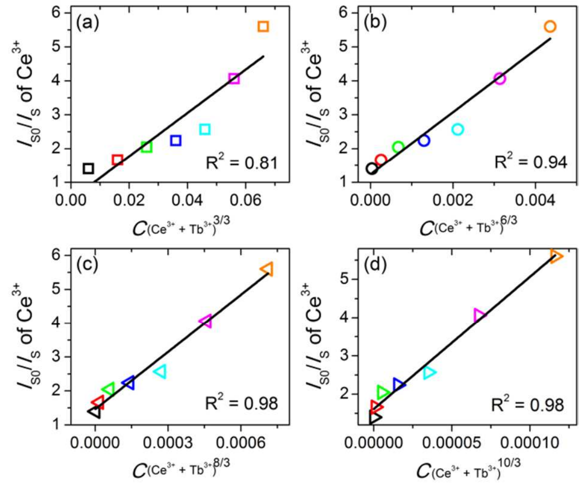

Figure 11. Dependence of I_{S0}/I_S of purplish-blue Ce^{3+} $C^{\alpha/3}$ in CBOF:0.03Ce^{3+}, yTb^{3+}, (0.03 + y)Na^+.

Table 1. Decay times of purplish-blue Ce^{3+} obtained from the decay curves

Tb^{3+} content	A_1	τ_1/ns	A_2	τ_2/ns	τ/ns	η(%)
0	918.56	26.0			26.0	
0.05	670.27	22.2	298.15	6.0	20.5	21.2
0.10	611.17	21.0	410.14	5.9	18.6	28.5
0.15	605.29	17.1	401.84	4.2	15.3	41.2
0.20	549.65	17.6	445.70	4.6	15.3	41.2
0.25	528.34	16.6	429.66	4.8	14.4	44.6
0.30	588.88	16.2	405.43	4.4	14.3	45.0

On the basis of Dexter's energy-transfer expressions of multi-polar interactions and Reisfeld's approximation, the energy transfer behavior from Ce^{3+} to Tb^{3+} can be deduced by the following formula[32, 33]

$$\eta_{S0}/\eta_S \propto C^{\alpha/3} \qquad (5)$$

where η_{S0} and η_S are the luminescence quantum efficiencies of Ce^{3+} in the absence and presence of Tb^{3+}, respectively; C is the total concentration of Ce^{3+} and Tb^{3+}; and the α values 3, 6, 8 and 10 correspond to exchange interaction, electric dipole-dipole (d-d), dipole-quadrupole (d-q) and quadruople-quadrupole (q-q) interactions, respectively. η_{S0}/η_S can be estimated approximately by the ratio of relative emission intensities (I_{S0}/I_S), where I_{S0} and I_S are the emission intensity of Ce^{3+} in the absence and presence of Tb^{3+}, respectively. Figure 11 shows the dependence of I_{S0}/I_S of purplish-blue Ce^{3+} on $C^{\alpha/3}$ in CBOF: 0.03Ce^{3+}, yTb^{3+}, (0.03 + y)Na^+. The linear relationship for I_{S0}/I_S - $C^{8/3}$ and I_{S0}/I_S - $C^{10/3}$ is better than the other two. However, q-q interaction is generally not expected to play an important role in solids in view of the very short interaction range.[34] Therefore, d-q interaction is responsible for the energy transfer from purplish-blue Ce^{3+} to Tb^{3+}.

The critical distance (R_c) of energy transfer from purplish-blue Ce^{3+} to Tb^{3+} can be calculated by using the equation given by Blasse[35]

$$R_c = 2[3V/(4\pi X_c N)]^{1/3} \qquad (6)$$

where V is the volume of the unit cell, N is the number of host cations in the unit cell. X_c is the total concentration of Ce^{3+} and Tb^{3+}, where the emission of Tb^{3+} in the co-doped phosphor reaches the maximum. By introducing the values of V (453.08 Å^3), N (10) and X_c (0.046, 0.03×0.2+0.20×0.2), the critical distance is calculated to be 12.3 Å, which is an effective distance for d-q interaction.

The PLE spectra in Figure 9 may suggest that the introduction of Tb^{3+} ion forces Ce^{3+} to occupy another Ca site and results in additional PLE and PL spectra. The PL spectra of Ce^{3+}, Tb^{3+} co-doped phosphors excited at 400 nm are illustrated in Figure 12a, which contain not only the emission peaks of Tb^{3+}, but also a broad band in 450-700 nm region peaking at ~530 nm. The emission intensities of both the broad band and Tb^{3+} peaks increase with Tb^{3+} content from 0.05 to 0.20, and then decrease. However, the PL intensities are much weaker than those based on purplish-blue emitting Ce^{3+}. The PL spectra of Ce^{3+}, Tb^{3+} co-doped samples excited by a 465 nm light are shown in Figure 12b, which also contain a broad band at ~540 nm. The broad band weakens and disappears with the increase of Tb^{3+} content. When monitored by 520 nm as containing little emission intensity from Tb^{3+}, the PLE spectra exhibit a strong band peaking at ~400 nm, a band at ~465 nm and several other weaker bands in the region of 200-370 nm (Figure 12c). The profile of the weaker bands is similar as that monitored at 541 nm (Figure 9b), which belongs to 4f → 5d transition of Tb^{3+} and purplish-blue Ce^{3+}. Sharp peaks on the 465 nm band are due to the interference of Xe lamp. The PLE bands at 400 and 465 nm have similar tendencies as those of the corresponding PL spectra. Figure 12d shows the PLE intensities versus Tb^{3+} content. All the luminescent properties shown before indicate that the co-doping of Tb^{3+} ions forces Ce^{3+} ions to occupy another Ca site, which results in a broad emission band at ~530 nm excited by a light around 400 nm. The PLE band at 465 nm and corresponding PL band at ~540 nm belong to CaO:Ce^{3+}, as these bands decrease with the increase of Tb^{3+}, which are in accordance with the XRD results.

Co-doping of Tb^{3+} ions facilitates the disappearance of CaO phase.

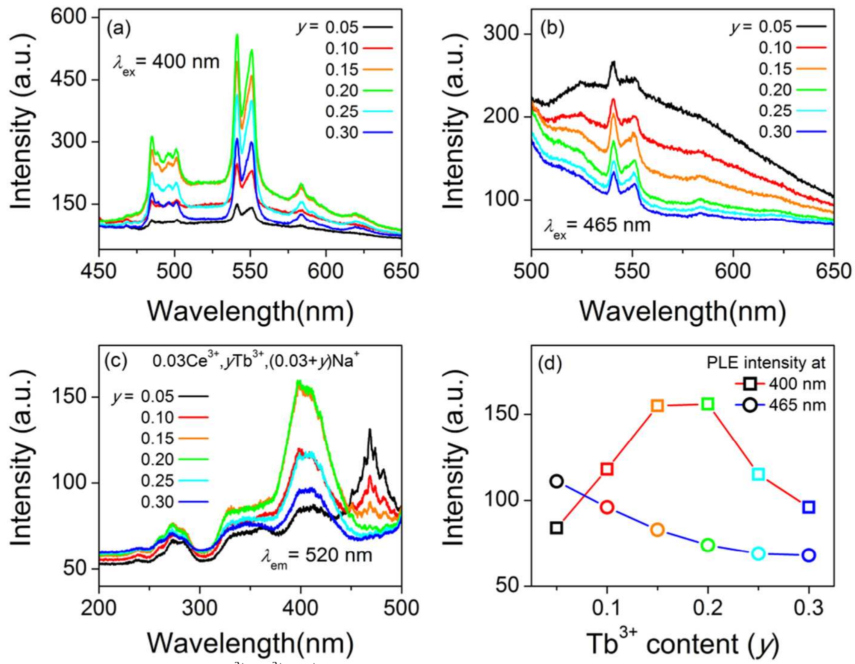

Figure 12. PL spectra of CBOF: Ce^{3+}, Tb^{3+}, Na^{+} excited by (a) 400 nm and (b) 465 nm light, (c) PLE spectra monitored at 520 nm, (d) PLE intensity at 400 and 465 nm versus Tb^{3+} content.

The above discussion indicates that Ce^{3+} ions can occupy two Ca sites of CBOF and exhibit two different luminescent properties. It is well known that the excitation and emission spectra of Ce^{3+} doped phosphors are related to nephelauxetic effect, crystal field splitting effect and Stokes shift.[36-38] The nephelauxetic effect will result in a shift of the energy barycenter (centroid shift, ε_c) of 5*d* levels relative to the free ion value. The crystal field splitting (ε_{cfs}) is the energy difference between the highest and lowest 5*d* levels of Ce^{3+} in a certain crystalline site. While Stokes shift is the energy difference between the peaks values of the lowest excitation band and the highest emission band.

The 5*d* centroid shift of Ce^{3+} (in eV, relative to the free ion value of 6.2 eV) can be expressed by the following equation[39, 40]

$$\varepsilon_c = 1.79 \times 10^{13} \sum_{i=1}^{N} \frac{\alpha_{sp}^{i}}{(R_i - 0.6\Delta R)^6} \quad (7)$$

where R_i is the distance (pm) between Ce^{3+} and anion *i* in the undistorted lattice. The summation is over all *N* anions that coordinate Ce^{3+}. $0.6\Delta R$ is a correction for lattice relaxation around Ce^{3+}, and ΔR is the difference between the radii of Ce^{3+} and cation sites that Ce^{3+} ions occupy. α_{sp}^{i} (in units of 10^{-30} m^{-3}) is the spectroscopic polarizability of anion *i*. For O, $\alpha_{sp}^{O} = 0.33 + 4.8/\chi_{av}^2$. For F, $\alpha_{sp}^{F} = 0.15 + 0.96/\chi_{av}^2$. χ_{av} is the electronegativity of the cations. $\chi_{av} = (10\chi_{Ca} + 9\chi_B)/19 = 1.47$ in $Ca_5(BO_3)_3F$, and one obtains $\alpha_{sp}^{O} = 2.55 \times 10^{-30}$ m^{-3} and $\alpha_{sp}^{F} = 0.59 \times 10^{-30}$ m^{-3}. If Ce^{3+} can occupy all the three Ca sites, the ε_c values for Ce^{3+}(1), Ce^{3+}(2) and Ce^{3+}(3) are calculated to be 1.52, 1.44 and 1.27 eV, respectively.

The energy of the lowest 5*d* excited level of Ce^{3+} is influenced by crystal field splitting and centroid shift. The crystal field splitting of the 5*d* levels can be expressed as[41]

$$\varepsilon_{cfs} = \beta_{poly}^{Q} R_{av}^{-2} \quad (8)$$

where β_{poly}^{Q} is a constant that depends on the type of the coordination polyhedron, Q is 3+ for Ce^{3+}, and R_{av} is close to the average distance between anions and cation~~s~~ that is replaced by Ce^{3+}. Three Ca sites are all coordinated by six anions. To simplify the comparison, the β_{poly}^{Q} values are assumed to be the same, viz. $\beta_{octa}^{Q} = 1.35 \times 10^9$ pm^2 cm^{-1}.[42] R_{av} values for Ca(1), Ca(2) and Ca(3) in $Ca_5(BO_3)_3F$ are 233.9, 241.5 and 235.6 pm, respectively. Therefore, the ε_{cfs} values for Ce^{3+}(1), Ce^{3+}(2) and Ce^{3+}(3) are 3.06, 2.87 and 3.02 eV, respectively. The ε_c and ε_{cfs} values for Ce^{3+}(1), Ce^{3+}(2) and Ce^{3+}(3) are in the following order:

ε_c: Ce^{3+}(1) > Ce^{3+}(2) > Ce^{3+}(3)

ε_{cfs}: Ce^{3+}(1) > Ce^{3+}(3) > Ce^{3+}(2)

Ca(2) is coordinated by six O atoms, forming an octahedron which is the most distorted one among the three Ca polyhedra. Ce^{3+} on an octahedron with a more distorted form may have more 5*d* sublevels. Therefore, it could be deduced that the PLE (360 nm) – PL (392 nm) spectra belong to Ce^{3+}(2). While PLE (400 nm) – PL (~530 nm) spectra may originate from Ce^{3+}(1) based on the comparison of ε_c and ε_{cfs}. Different Stokes shift values are related to the difference in size and morphology of the Ca sites occupied by Ce^{3+}. The 4*f* and 5*d* energy levels of Ce^{3+} on the two Ca sites and energy transfer from Ce^{3+} to Tb^{3+} are illustrated roughly in Figure 13.

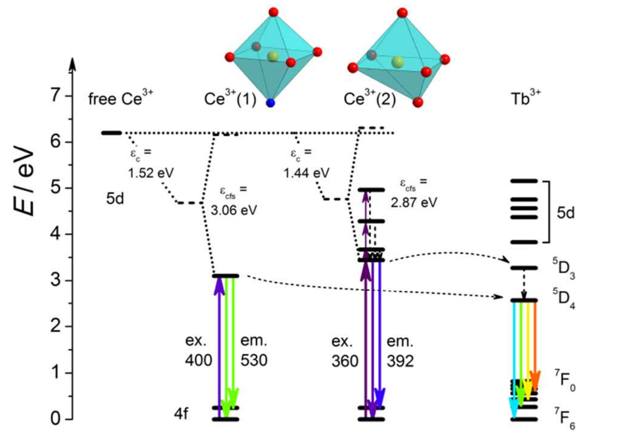

Figure 13. Schematic diagram of 4*f* and 5*d* energy levels for Ce^{3+} and Tb^{3+}, and $Ce^{3+} \rightarrow Tb^{3+}$ energy transfer in CBOF host.

4. Conclusion

In summary, Ce^{3+} doped and Ce^{3+}, Tb^{3+} co-doped $Ca_5(BO_3)_3F$ phosphors have been synthesized successfully by a high-temperature solid-state reaction. $Ca_5(BO_3)_3F$: Ce^{3+}, Na^+ phosphor exhibits a purplish-blue emission peaking at 392 nm with a strongest excitation band at 360 nm, which originates from Ce^{3+} on Ca(2) site. The excitation energy of Ce^{3+} can transfer to Tb^{3+} efficiently, showing a broader excitation band in 300-400 nm region for Tb^{3+}. Furthermore, the co-doping of Tb^{3+} ion results in the appearance of green emitting Ce^{3+} on Ca(1) site. Ce^{3+}, Tb^{3+} co-doped $Ca_5(BO_3)_3F$ shows potential application as green emitting phosphor for near-UV LEDs.

Acknowledgements

This work was financially supported by the National Natural Science Foundation of China (grant no. 51402105 and 21471055), Specialized Research Fund for the Doctoral Program of Higher Education (grant no. 20134306120009 and 20124306120005), Hunan Provincial Natural Science Foundation of China (grant no. 12JJ2029) and Aid Program for Science and Technology Innovative Research Team in Higher Educational Institutions of Hunan Province.

References

1 L. Chen, C.-C. Lin, C.-W. Yeh and R.-S. Liu, *Materials*, 2010, **3**, 2172-2195.
2 C. C. Lin and R.-S. Liu, *J. Phys. Chem. Lett.*, 2011, **2**, 1268-1277.
3 P. F. Smet, A. B. Parmentier and D. Poelman, *J. Electrochem. Soc.*, 2011, **158**, R37-R54.
4 V. Bachmann, C. Ronda and A. Meijerink, *Chem. Mater.*, 2009, **21**, 2077-2084.
5 S. Ye, F. Xiao, Y. X. Pan, Y. Y. Ma and Q. Y. Zhang, *Mater. Sci. Eng. R*, 2010, **71**, 1-34.
6 M. Shang, C. Li and J. Lin, *Chem. Soc. Rev.*, 2014, **43**, 1372-1386.
7 Z. Xia, Y. Zhang, M. S. Molokeev, V. V. Atuchin and Y. Luo, *Sci. Rep.*, 2013, **3**, 3310.
8 Y. He, J. Zhang, W. Zhou, J. Han, Z. Qiu, L. Yu, C. Rong and S. Lian, *J. Am. Ceram. Soc.*, 2014, **97**, 1517-1522.
9 S.-P. Lee, C.-H. Huang, T.-S. Chan and T.-M. Chen, *ACS Appl. Mater. Interfaces*, 2014, **6**, 7260-7267.
10 A. Kalaji, M. Mikami and A. K. Cheetham, *Chem. Mater.*, 2014, **26**, 3966-3975.
11 W.-Y. Huang, F. Yoshimura, K. Ueda, Y. Shimomura, H.-S. Sheu, T.-S. Chan, C.-Y. Chiang, W. Zhou and R.-S. Liu, *Chem. Mater.*, 2014, **26**, 2075-2085.
12 X. Gong, J. Huang, Y. Chen, Y. Lin, Z. Luo and Y. Huang, *Inorg. Chem.*, 2014, **53**, 6607-6614.
13 M. Jiao, Y. Jia, W. Lu, W. Lv, Q. Zhao, B. Shao and H. You, *Dalton Trans.*, 2014, **43**, 3202-3209.
14 Y. Li, Y. Shi, G. Zhu, Q. Wu, H. Li, X. Wang, Q. Wang and Y. Wang, *Inorg. Chem.*, 2014, **53**, 7668-7675.
15 X. Zhang, L. Zhou, Q. Pang, J. Shi and M. Gong, *J. Phys. Chem. C*, 2014, **118**, 7591-7598.
16 X. Zheng, H. Luo, J. Liu, P. Liu and X. Yu, *J. Mater. Chem. C*, 2013, **1**, 7598-7607.
17 Y. Zhang, G. Li, D. Geng, M. Shang, C. Peng and J. Lin, *Inorg. Chem.*, 2012, **51**, 11655-11664.
18 Z. Xia and R.-S. Liu, *J. Phys. Chem. C*, 2012, **116**, 15604-15609.
19 G. Li, Y. Zhang, D. Geng, M. Shang, C. Peng, Z. Cheng and J. Lin, *ACS Appl. Mater. Interfaces*, 2012, **4**, 296-305.
20 H. Liu, Y. Luo, Z. Mao, L. Liao and Z. Xia, *J. Mater. Chem. C*, 2014, **2**, 1619-1627.
21 D. Geng, M. Shang, Y. Zhang, H. Lian, Z. Cheng and J. Lin, *J. Mater. Chem. C*, 2013, **1**, 2345-2353.
22 J. Chen, Z. Xia and Q. Liu, *J. Mater. Chem. C*, 2015, **3**, 4197-4204.
23 Z. Xia, J. Zhuang, A. Meijerink and X. Jing, *Dalton Trans.*, 2013, **42**, 6327-6336.
24 G. Zhu, S. Xin, Y. Wen, Q. Wang, M. Que and Y. Wang, *RSC Adv.*, 2013, **3**, 9311-9318.
25 Y. Wang, M. G. Brik, P. Dorenbos, Y. Huang, Y. Tao and H. Liang, *J. Phys. Chem. C*, 2014, **118**, 7002-7009.
26 M. Jiao, N. Guo, W. Lü, Y. Jia, W. Lv, Q. Zhao, B. Shao and H. You, *Inorg. Chem.*, 2013, **52**, 10340-10346.
27 C. D. Wagner, W. M. Riggs, L. E. Davis, J. F. Moulder and G. E. Muilenberg, *Handbook of X-ray Photoelectron Spectroscopy*, Perkin-Elmer Corporation and Physical Electronics Division, Eden Prairie, 1979.
28 Z. Hao, X. Zhang, Y. Luo, L. Zhang, H. Zhao and J. Zhang, *J. Lumin.*, 2013, **140**, 78-81.
29 Z. Hao, X. Zhang, X. Wang and J. Zhang, *Mater. Lett.*, 2012, **68**, 443-445.
30 C.-H. Huang and T.-M. Chen, *J. Phys. Chem. C*, 2011, **115**, 2349-2355.
31 P. I. Paulose, G. Jose, V. Thomas, N. V. Unnikrishnan and M. K. R. Warrier, *J. Phys. Chem. Solids*, 2003, **64**, 841-846.
32 D. L. Dexter, *J. Chem. Phys.*, 1954, **22**, 1063-1070.
33 R. Reisfeld, E. Greenberg, R. Velapoldi and B. Barnett, *J. Chem. Phys.*, 1972, **56**, 1698-1705.
34 C. Ronda, *Luminescence: From Theory to Applications*, WILEY-VCH Verlag GmbH & Co. KGaA, Weinheim, 2008.
35 G. Blasse, *Philips Res. Rep.*, 1969, **24**, 131-144.
36 V. Bachmann, C. Ronda, O. Oeckler, W. Schnick and A. Meijerink, *Chem. Mater.*, 2009, **21**, 316-325.
37 G. Blasse and B. C. Grabmaier, *Luminescent Materials*, Springer-Verlag, Berlin, 1994.
38 R.-J. Xie, Y. Q. Li, N. Hirosaki and H. Yamamoto, *Nitride Phosphors and Solid-State Lighting*, Taylor & Francis, Boca Raton, 2011.
39 P. Dorenbos, *Phys. Rev. B*, 2000, **62**, 15640-15649.
40 P. Dorenbos, *J. Lumin.*, 2003, **105**, 117-119.
41 P. Dorenbos, *J. Phys.-Condens Mat.*, 2003, **15**, 4797-4807.
42 P. Dorenbos, *Phys. Rev. B*, 2001, **64**, 125117.